24th Applied Aerodynamics Conference
5 - 8 June 2006, San Francisco, California

AIAA 2006-3660

The Application of Variable Cant Angle Winglets for Morphing Aircraft Control

P. Bourdin*, A. Gatto*, and M.I. Friswell†

University of Bristol, Bristol, England BS8 1TR, United Kingdom

This paper investigates a novel method of control for 'morphing' aircraft. The concept consists of a pair of winglets with adaptive cant angle, independently actuated, mounted at the tips of a flying wing. Computations with a vortex lattice model and wind tunnel tests demonstrate the validity of the concept. The variable cant angle winglet appears to be a multi-axis effector with a favorable coupling in pitch and roll with regard to turning manoeuvres.

Nomenclature

α	angle of attack
δ_e	elevator deflection angle
η	reduced spanwise coordinate
Γ	vortex strength
γ_l, γ_r	left and right winglet cant angles
Γ_x	vortex strength sensitivity w.r.t. variable x
Ω	turn rate
ϕ	bank angle
ρ	air density
b	wing span
C_D, C_Y, C_L	drag, side-force and lift coefficients
C_l, C_m, C_n	rolling, pitching and yawing moment coefficients
C_{D_x}, C_{Y_x}, C_{L_x}	drag, side-force and lift coefficient derivatives w.r.t. parameter x
C_{l_x}, C_{m_x}, C_{n_x}	rolling, pitching and yawing moment coefficient derivatives w.r.t. parameter x
c_{root}	root chord
g	gravitational acceleration
p, q, r	aircraft rotation rates in body or stability axes
R	turn radius
u, v, w	aircraft velocity components in body or stabilty axes
V_{cg}	flight speed
W	aircraft weight
CG	center of gravity
LE	leading edge
TE	trailing edge

I. Introduction

Since the dawn of powered flight more than one hundred years ago, aircraft designers have sought to improve on existing aircraft control methodologies. In those early years, structural compliance techniques were actively built into aircraft structures as a means of controlling the aircraft with the most notable

*Research Associate, Dept. of Aerospace Engineering.
†Professor, Dept. of Aerospace Engineering.

technique being the ingenious "wing warping" employed by the Wright brothers for roll control.[1] Since that time, a gradual progression in aircraft control systems has seen a shift from these compliant based techniques to the currently used and widely accepted techniques of strategically placed, small deflection, discrete control surfaces. As successful as these present methods have been over the last century, aircraft designers, faced with the challenging needs of 21st century air forces, must now confront challenges that only a radical re-think in current aircraft design thinking can hope to overcome. Paramount to these challenges is the requirement for any future flight vehicle to possess the ability to perform and execute, multiple, dissimilar mission roles and objectives. These can include a dual low subsonic and supersonic flight speed capability, extraordinary agility and control authority and advanced anti-detection systems.

Some of the more current morphing wing/aircraft concepts have dealt with aspects of flight control and/or multiple mission adaptability.[2–9] Morphing for flight control involves primarily, small, continuous adjustments in the shape of the wing[3–5] and/or surrounding flowfield[6] to manoeuvre the aircraft during flight. Morphing for mission adaptation involves making greater shape changes in order to optimize, in flight, the wing characteristics for the current flight condition.[7–9]

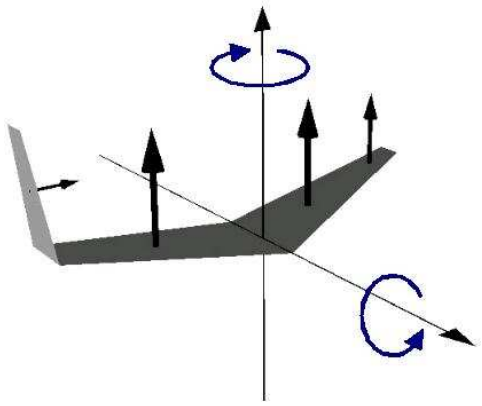

Figure 1. An unsymmetric wing-tip arrangement for a sweptback wing to initiate a coordinated turn.

In this paper, we take the view of morphing for control, investigating a concept using independently controllable articulated winglets on a flying wing model to achieve basic manoeuvres. Using variable cant angle winglets on this particular configuration allows the symmetry of the wing relative to its longitudinal plane to be broken through the differential and unsymmetric movement of the left and right-hand-side winglets. This allows control of both the lateral and directional balance of the model. For example, with the left winglet planar to the wing plane and the right winglet rotated at a positive cant angle (i.e. pointing upward), the model will experience a positive rolling moment (right wing goes down) due to the reduction in lift from the right wing. A positive yawing moment (right wing moves aft) is also experienced by the model due to the inward side-force generated by the right winglet, located aft of the model centre of gravity. Since the yawing moment is in the same direction as the intended roll (proverse yaw), a coordinated turn should then be achievable by adjusting the magnitude of one moment relative to the other. This idea of manoeuvring using articulated winglets is illustrated in figure 1. Additional effects due to the rotation of the right winglet include a negative yaw moment due to the drag increase on the left wing (more lift means more drag) and a negative rolling moment due to the sideforce acting above the wing center of gravity, but these will be found to be an order of magnitude lower than the roll and yaw control moments.

The paper is organized as follows: Section II describes the flying wing model we selected to investigate the suitability of the variable-cant-angle winglet concept for effective aircraft control. Sections III and IV give an overview of the numerical and experimental methods we relied on to analyze this concept. Presentation and discussion of the numerical and experimental results are done in section V, and conclusions are drawn in section VI.

II. Characteristics of the Investigated Airframe

A. Geometry

The model used for experimental testing was constructed from a commercially available flying wing made from EPP foam. The unmodified, baseline configuration consisted of a trapezoidal planar wing with 30^o LE sweep, with aspect and taper ratios of 4.6 and 0.56 respectively. The wing was untwisted and lofted with a 12% thick zagi airfoil section (which exhibits a reflexed TE, see figure 2). Modifications to this baseline configuration were primarily performed at the wing tips through the addition of servo-driven articulated hinges where the adaptive winglets were fixed. The assembly of the wing/winglet interface conserved the LE and TE sweep angles of the entire configuration. Experimentally, only one winglet length has been considered, which represented 50% of the baseline semispan; numerically however, a shorter winglet length

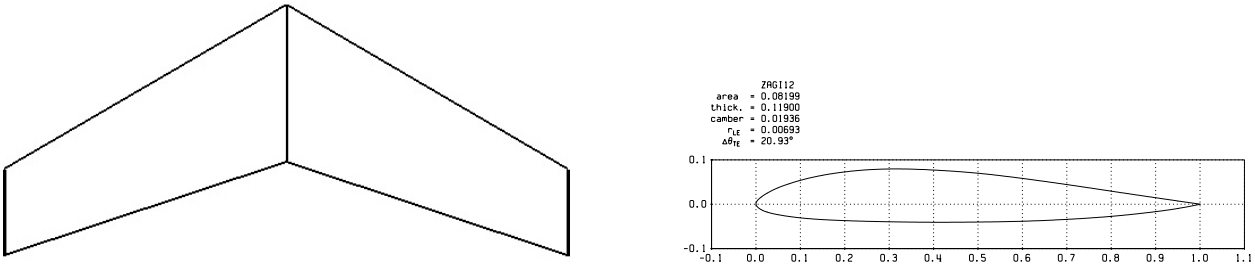

Figure 2. Baseline configuration planform and airfoil section.

Figure 3. Experimental model as mounted in the wind-tunnel; left: both winglets planar; right: both winglets upright.

has also been analyzed, which represented 25% of the baseline semispan. In the remainder of this paper, the longer winglets will be referred to as "long winglets", and the shorter ones as "short winglets". The experimental model, featuring the long winglets, is shown in figure 3.

Remark: One could argue here that such a hinged winglet is yet another conventionally-actuated, discrete control surface and therefore do not constitute some morphing object according to the definition given in the introduction of this paper, but bear in mind that we are still in the early design phase and therefore the model presented here serves rather as a proof-of-concept. Once proven valid, one can spend more time improving the prototype such as to provide for example a continuous "span camber" change instead of a wing/winglet combination.

B. Control Allocation Scheme

The baseline configuration was fitted with a pair of elevons (lying from $\eta = 0.08$ to $\eta = 1$) as primary pitch and roll control effectors. After addition of the adaptive winglets, these elevons were used only as elevators (i.e. symmetrically deflected) to provide primary pitch control or longitudinal trimming, and the independently-actuated winglets were used as primary yaw and roll control effectors, except in cases reported in §V.C where both the winglets were symmetrically deflected so as to provide control and trim in pitch.

III. Experimental Setup and Apparatus

The model was installed inside a closed test section, closed circuit wind tunnel whose maximum operating freestream velocity was 60 m/s. The freestream velocity chosen for this investigation was 10 m/s, giving a Reynolds number of 1.83×10^5 based on the mean aerodynamic chord of the baseline configuration (2.30×10^5

based on the root chord). The freestream turbulence level at the model station was approximately 0.2%. The model was mounted at mid-height in the test section, on top of a support strut connecting the model to a high-frequency, dynamic load cell mounted to the underside of the floor of the test section. Access to the wind tunnel test section for the support strut was provided by a cutout in the wind tunnel floor which was covered, during wind tunnel testing, by two thin sheets of fibreboard. Each sheet was constructed to ensure no contact between the supporting strut and the test section was possible. Four high-tension wires were also installed between the active balance plate and the top of the support strut to increase the stiffness of the entire support system thereby improving the natural frequency characteristics of the combination.

Force and moment data obtained from the model were acquired using a JR3, multi-axis load cell in combination with conditioning electronics and a DAQ card installed in a PC. Calibration of the load cell conducted prior to wind-on test conditions indicated an error in the reading of all forces and moments to be better than $\pm 5\%$. Estimates of the static support tare for all six degrees of freedom were also obtained prior to wind tunnel tests with all data presented hereafter corrected for these results.

All four servos used to control the model were driven by a dSPACE control system. This system was configured to generate pulse width modulated input signals (50 Hz) with variable duty cycles corresponding to a pulse width range of between 900-2100 μs (center position 1500 μs). Calibration of the control surface position was carried out using a digital inclinometer (error $\pm 0.1^o$) positioned on the control surfaces and matched to a readout from the dSPACE control system indicating the input signal pulse width. Achievable cant angle [a] magnitudes for the winglets and deflection magnitudes for the elevons were -90^{o}to 90^o (0^o planar) and -30^o to 30^o respectively. The same digital inclinometer was used to calibrate the angle of attack of the model which was measured relative to a flat, prefabricated cut-out at the mid-plane of the wing, co-incident with the chord line.

Preliminary results presented in this paper focus on the effect of modifying the cant angle at fixed angles of attack. Unless stated otherwise, elevons were set to neutral.

IV. Numerical Method

To provide performance and stability estimates, we rely on a vortex lattice representation of the wing: the lifting surfaces and their trailing wakes are modeled as a discrete set of horseshoe vortex filaments stacked along the span and chord axes. The vortex strengths (yielding the discrete spanwise and chordwise loading) are obtained as the solution of a system of linear equations that enforce a flow-tangency condition at specified control points on the wing. All the horseshoe vortices belonging to the same spanwise strip are co-planar, so the sectional camber and the deflection of any conventional LE/TE control surfaces are modeled by tilting the normal vector of the relevant panels when applying the flow-tangency boundary condition. Because large winglet deflections will be investigated, winglet deflections are handled by truly deflecting the aerodynamic grid. The forces and moments are obtained from the solved vortex strengths by making use of the Kutta-Joukowsky theorem [10, pp. 46–48] over all the bound vortex segments:

$$d\vec{F} = \rho \vec{V} \times \Gamma d\vec{l} \tag{1}$$

where $\vec{V}$ is the total velocity (translation + rotation + induced velocities) at the centroid of vortex segment of length dl, $d\vec{F}$ is the force acting on that infinitesimal segment.

Provided that the dimensionless rotation rates and reduced frequencies are slow enough, any unsteady vortex shedding and wake deformation effects can be legitimately overlooked so that the previous steady-state aerodynamic model can be used to predict the instantaneous performance and quasi-static stability derivatives during a rotary or oscillatory motion of the wing.

As regards the adaptive winglets, the corresponding control derivatives are obtained from finite differences by perturbating the aerodynamic grid. Otherwise, stability derivatives are computed during the vortex strength solution procedure, as follows: the linear system enforcing the flow tangency is solved in turn for a unit airframe velocity (linear or angular) along each Cartesian axis, yielding the sensitivities of the vortex strengths with respect to that velocity component as solution. Then the sensitivities with respect to the angles of LE/TE control surfaces (in our case, a pair of elevators) are computed in a similar manner by enforcing in turn a unit deflection of each control surface for the desired values of the airframe linear and

[a] In the paper, we define the cant angle as the dihedral angle formed by the winglet with the wing plane. It is positive for up winglet.

angular velocities. For the desired values of the operating variables (linear and angular velocities, u, v, w, p, q, r, plus deflection angles of the LE/TE control surfaces – elevator deflection δ_e in our case), the vortex strengths are then readily obtained from (2) since their governing equations are linear.

$$\Gamma = u\Gamma_u + v\Gamma_v + w\Gamma_w + p\Gamma_p + q\Gamma_q + r\Gamma_r + \delta_e\Gamma_{\delta_e} \tag{2}$$

The vortex strengths along with their sensitivities being now known, the static derivatives can then be obtained by summing the differentiated Kutta-Joukowsky theorem (with respect to the airframe linear and angular velocity components and the control deflections) all over the wing horseshoe vortices.

This inviscid aerodynamic model is corrected for viscous drag (with regard to force, moment and stability derivative computations) by using a section-lift dependent, parabolic, airfoil drag polar model.

V. Results and Discussion

In the results presented hereafter the following conventions apply:

- moments are referenced about the CG of the analyzed configuration;
- rolling and yawing moments were made dimensionless using the span of the planar configuration as reference length;
- the mean aerodynamic chord (m.a.c.) was used as the reference length for the pitching moment;
- moments are given in the standard stability axes (x forward, y to the right of the pilot, z down) and taken positive according to the right-hand rule about those axes.

A. Effect of moving winglets on flight dynamics

Since winglets are rotated about an axis parallel to the wing-center chord line, the chordwise location of the airframe center of gravity remains unchanged during this transformation. Only its spanwise location (if right and left deflection angles have different magnitudes) and vertical location will change. Those changes for our flying wing model equipped with long winglets are shown in figure 5. Note that they are rather unsignificant due to the small weight of the winglet relative to the whole wing ($W_{winglet}/W_{wing} = 3\%$). Contrary to the CG chordwise location, the chordwise location of the wing aerodynamic center will change when one or both winglets are rotated (either downward or upward): as shown in figure 6 for the long-winglet case, the more the winglet is deflected off the wing plane, the further ahead the aerodynamic center is relocated (relative to the planar configuration, a forward displacement representing 7% of the root chord is predicted when one winglet is upright at $\pm 90^o$ while the other one is planar, this is roughly doubled when both winglets are deflected). This forward displacement reduces the static margin and hence the pitch stiffness (C_{m_α}), which allows some potential for controlling or trimming the aircraft longitudinally (see figure 4). To maintain the static longitudinal stability over the range of permitted cant angles ($-90^o \rightarrow +90^o$), the longitudinal position of the CG has been fixed so as to get a static margin of at least +5% (based on the mean aerodynamic chord of the planar configuration) when the aerodynamic center lies at its foremost position (i.e. when the cant angle is $\pm 90^o$). Unless stated otherwise, the longitudinal position of the CG was located:

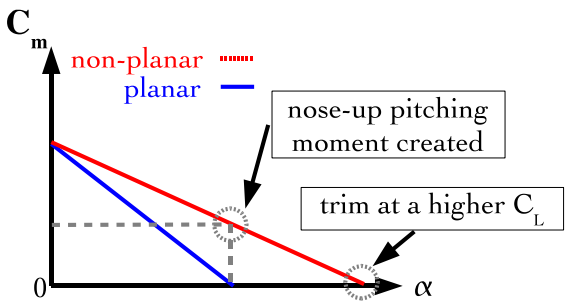

Figure 4. Effect of folding tips on pitch: when one or both tips of the trimmed, longitudinally stable, planar configuration are folded up or down at fixed angle of attack, a nose-up pitching moment is created (aerodynamic center jumps forward while CG is fixed ⇒ reduced static margin ⇔ C_{m_α} is less negative). If the angle of attack is allowed to be adjusted, one can then trim at a larger C_L.

- 0.76 c_{root} aft of the wing apex in the long-winglet case when only one winglet at a time was allowed to be deflected off the wing plane;

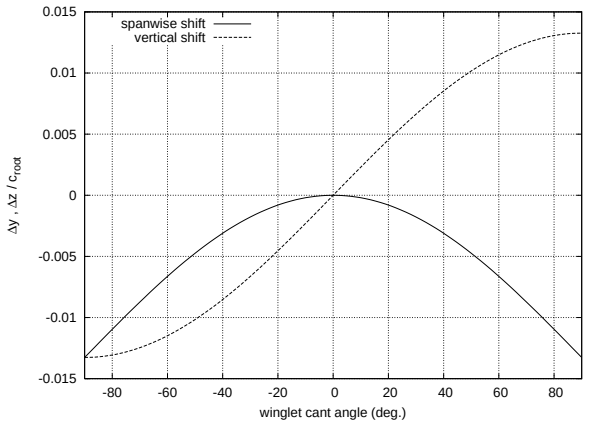

Figure 5. Variation of the CG locus in the lateral plane when right winglet is rotated while left winglet remains planar (long-winglet case, offsets are relative to the fully planar configuration and normalized by the root chord).

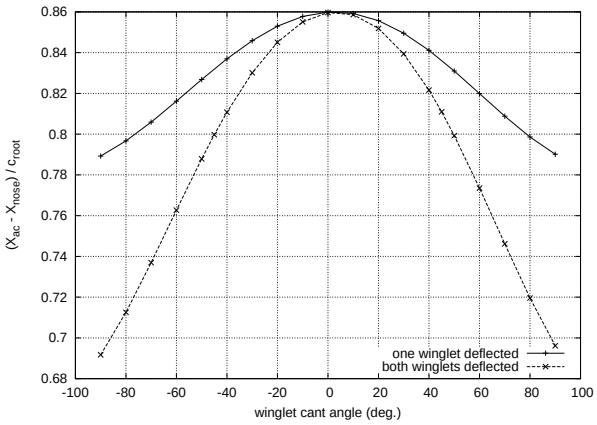

Figure 6. Longitudinal locus (relative to the wing apex, X body axis aft) of the wing aerodynamic center when one or both winglets are deflected off the wing plane (long-winglet case, VLM computations with neutral elevator, positive cant angle is winglet up).

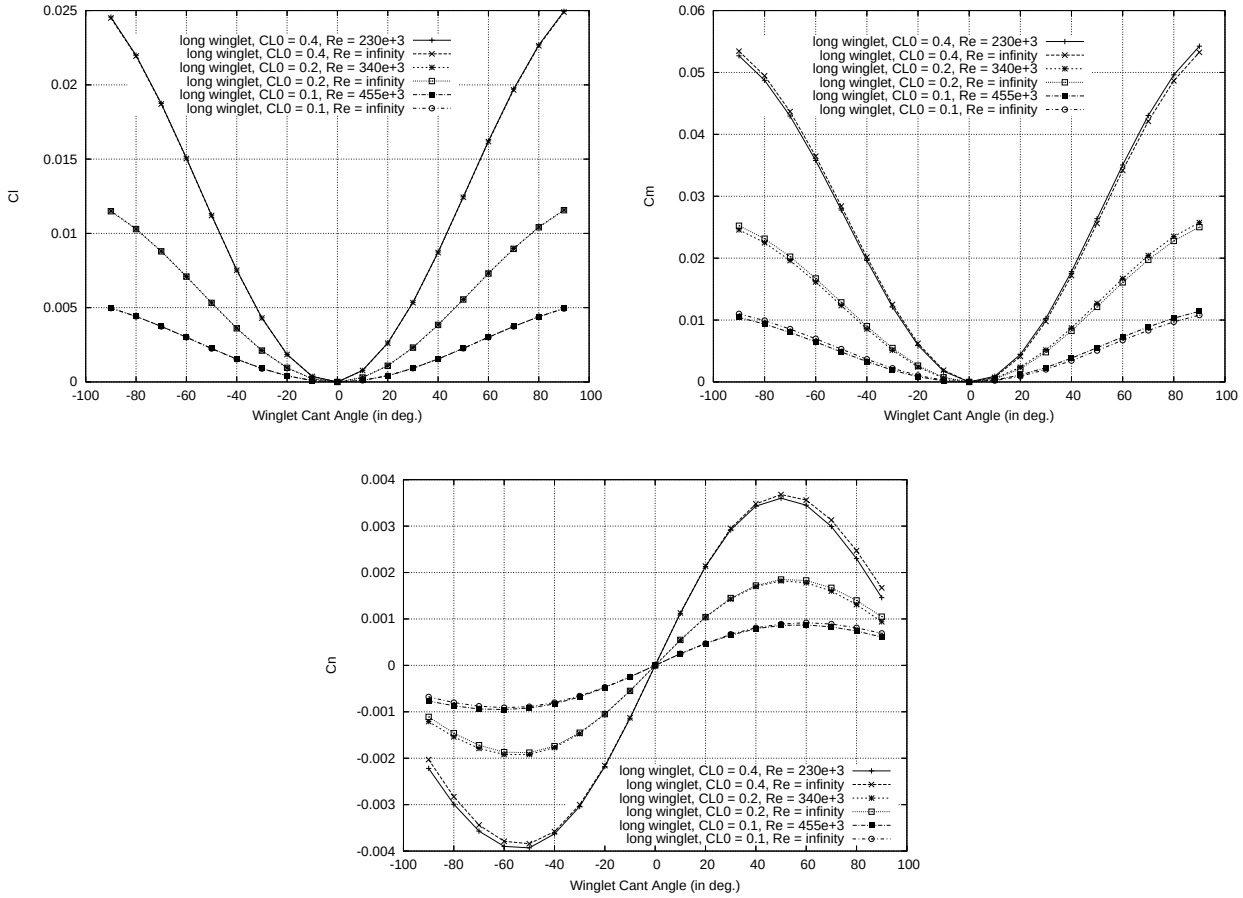

Figure 7. Moments attainable by folding up or down the right winglet while the left one remains planar (numerical predictions for the long-winglet case; $Re \to \infty$ means the profile drag has not been accounted for during the computations; a finite Re value means the results have been corrected for profile drag effects at that Reynolds number; Re values are based on the root chord and on the flight speeds at sea level corresponding to the prescribed reference lift coefficient C_{L_0}).

- 0.65 c_{root} aft of the wing apex in the long-winglet case when winglets were allowed to be deflected in tandem;
- 0.69 c_{root} aft of the wing apex in the short-winglet case when only one winglet at a time was allowed to be deflected off the wing plane;
- 0.65 c_{root} aft of the wing apex in the short-winglet case when winglets were allowed to be deflected in tandem.

B. Application to lateral/directional control and balance: winglets deflected apart

From a steady symmetric level flight with both winglets planar, we want to roll the wing into a steady, coordinated turn (say to the right, to be consistent with the example depicted in figure 1). This is a two-step process involving first the creation of a rolling moment to initiate the turn (in the present case, by raising the right winglet and leaving the left one planar), and then the trimming of the rolling, pitching and yawing moments to sustain the turn.

1. Attainable moments

Rolling, pitching and yawing moments were computed at fixed angle of attack and fixed elevator angle, Those angles corresponded to a trimmed, symmetric, level flight state of the configuration with undeflected winglets (such a trimmed state for the planar configuration was obtained by the VLM code by adjusting iteratively the angle of attack and elevator angle so as to zero out the pitching moment and to obtain a prescribed lift coefficient). Three trimmed reference states were considered, corresponding to the following prescribed lift coefficients for the planar configuration: $C_{L_0} = 0.4\,;\, 0.2\,;\, 0.1$ (all the coefficients mentioned in the remainder of the paper are based on the reference area of the configuration with undeflected winglets, even for the non-planar, non-symmetric configurations). Numerical results corresponding to a cant-angle sweep at each of those fixed (α, δ_e) pairs are plotted in figure 7, note that taking or not the profile drag into account does not involve much change in the computed moments. As expected, a positive rolling control moment is produced, that is the wing will roll to the right (i.e. to the side where the winglet is deflected), whether the winglet is deflected up or down (curves are nearly symmetric w.r.t. cant angle). One can also notice a positive side-effect of the winglet deflection on the pitching moment: a nose-up pitching moment is created, as explained in figure 4, which is desired to achieve a level turn and may thus alleviate the use of elevators. With up winglet, a yaw moment in the same direction as the intended roll appears (due to the winglet inward sideforce acting aft of the wing CG), which will point the aircraft nose into the intended turn and is therefore a proverse effect. On the opposite, down winglet yields an adverse yaw moment. Note that, unlike the pitching and rolling moments, maximum yawing moments do not occur at maximum winglet deflection (i.e. $\pm 90^o$) but about 50^o cant angle.

It appears that up winglet is to be used to initiate a turn with minimum adverse effects direction-wise, however the generated yaw moments are one order of magnitude smaller than the generated roll moments and since the inertia moments about the vertical and lateral axes are roughly the same for a flying wing, the resulting angular acceleration in yaw will also be smaller by one order of magnitude compared to the angular acceleration in roll, therefore the adverse yaw with down winglets may not be too significant in our case. Configurations featuring the short winglets were also analyzed via the VLM. Results (not shown here) are similar but halved in magnitude, which indicates that the generated moments are proportional to the winglet length. The previous numerical results for the long winglets are compared to wind tunnel data in figure 8, for the cases $C_{L_0} = 0.2\,;\, 0.4$. Measured and predicted aerodynamic moments are given about the same reference point (the CG location used in the numerical work). In contrast with the numerical investigation, elevators were set to neutral (aeroelastic effects warped them though) during the experimental investigation, but that should not be a significant source of discrepancy between computational and experimental results since the deflection angles used in the numerical simulations were of a few degrees only. As a matter of fact the predicted rolling and yawing moments are in good agreement with the measured ones except for large winglet deflections in the case $C_{L_0} = 0.2$, where the VLM under-predicted the measured moments. In terms of pitching moments, the agreement between simulation and experiment is not as good (to make the comparison easier, the pitching moment value measured for the planar configuration was subtracted to all the measured pitching moments, because the planar configuration was not trimmed in pitch during the tests, but it was during the numerical simulations): the experimental data appear to be a bit offset, relative

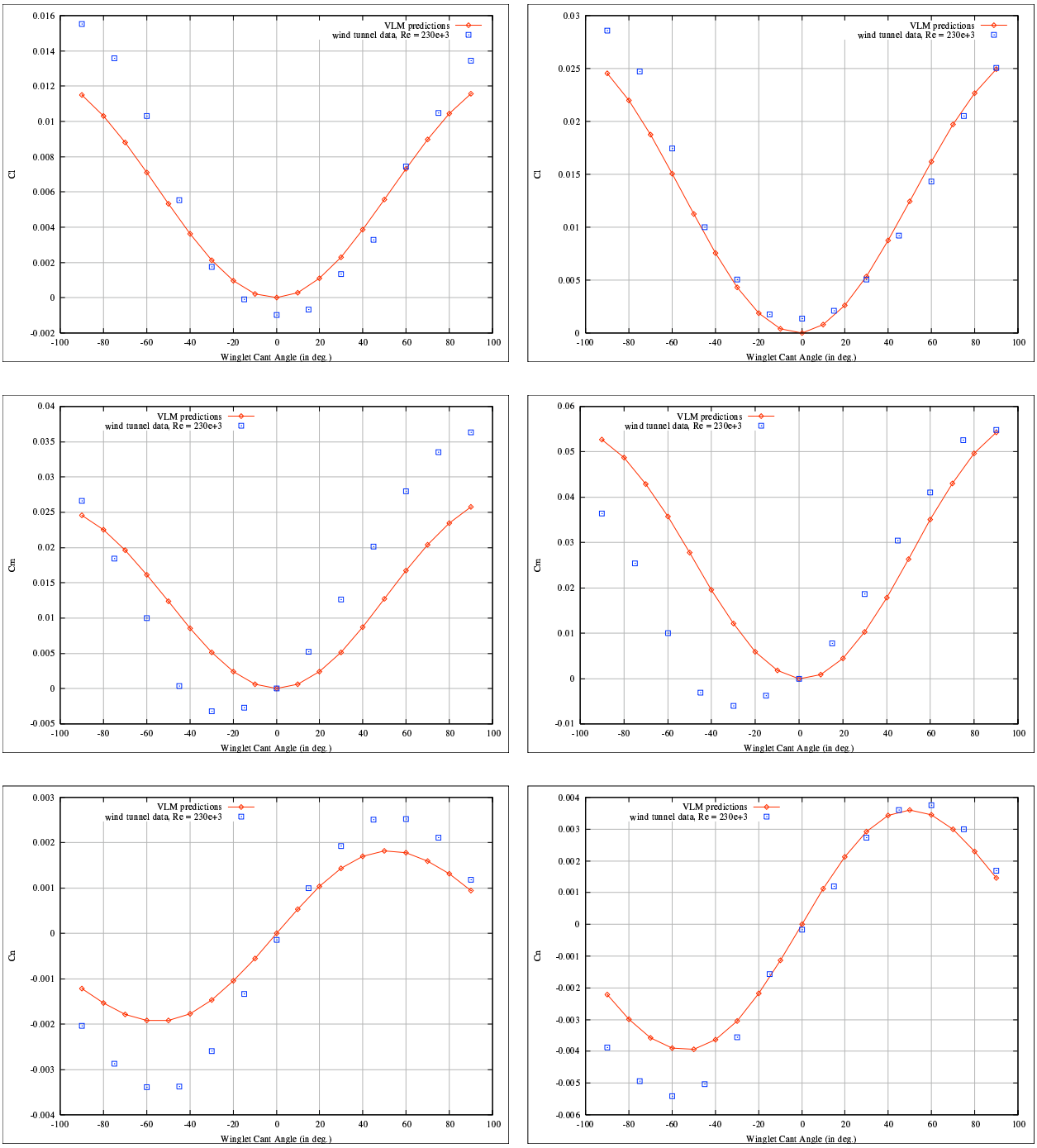

Figure 8. Moments attainable by folding up or down the right winglet while the left one remains planar (VLM predictions corrected for profile drag and wind tunnel data; long-winglet case; from top to bottom: C_l, C_m, C_n; left column: $C_{L_0} = 0.2$; right column: $C_{L_0} = 0.4$; Re displayed for experimental data is based on root chord).

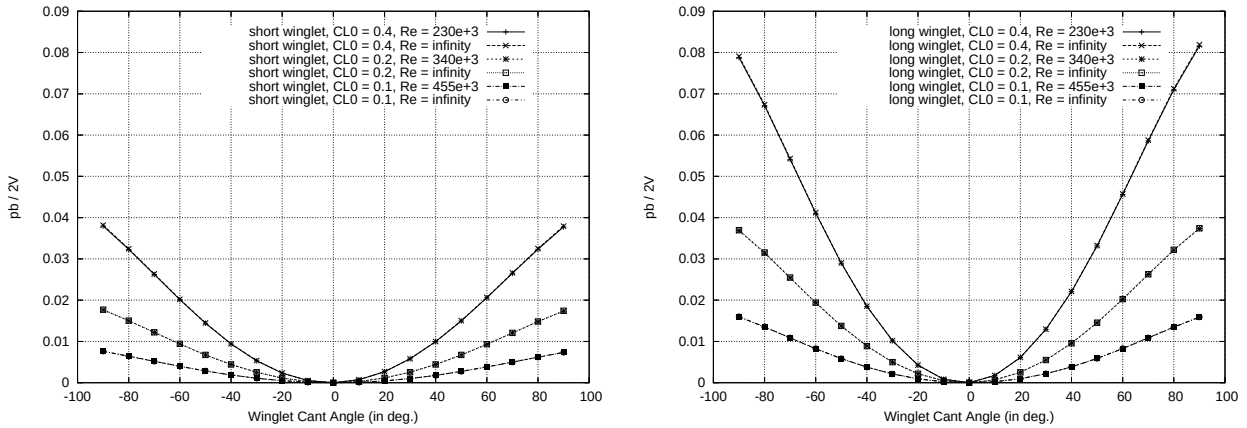

Figure 9. Steady-state roll rate attainable by folding up or down the right winglet while the left one remains planar (right: numerical predictions for the short-winglet case; left: numerical predictions for the long-winglet case; $Re \to \infty$ means the profile drag has not been accounted for during the computations; a finite Re value means the results have been corrected for profile drag effects at that Reynolds number; Re values are based on the root chord and on the flight speed at sea level corresponding to the cruise lift coefficient C_{L_0} upon initiation of the roll).

to the numerical ones, towards the negative cant angles. This unsymmetry appearing in the measured pitching moment versus cant angle curves may be ascribed to the flexibility of the structure (in particular, the elevators) which suffered from significant, unsymmetric aeroelastic effects during the tests (certainly magnified by the unsymmetric arrangement of the winglets).

2. Steady-state roll rate

The winglet effectiveness in producing roll is the key parameter during the first step of the turn manoeuvre. One can assess this effectiveness by estimating the achievable roll rate, assuming a single degree-of-freedom in the equations governing the rotary motion of the wing. Solving for the steady state gives: $\hat{p} = -C_{l_0}/C_{l_p}$, where $\hat{p} = pb/2V_{cg}$ is the dimensionless roll rate, C_{l_0} is the rolling moment that initiated the roll (rolling moment due to the rotation of the right winglet), and C_{l_p} is the damp-in-roll derivative about the state that initiated the roll. Numerical results for the short and long winglets, and three different lift coefficients upon initiation of the roll are plotted against the cant angle in figure 9. C_{l_0} and C_{l_p} were obtained on the basis of steady-state aerodynamics using the VLM code (as in §V.B.1): the wing with right winglet deflected at the desired cant angle was analyzed with zero rotation speed at the angle of attack and elevator angle of the trimmed, symmetric, level flight state. The results show that the roll rate does not depend on the cant angle sign (i.e. whether the winglet is up or down), and is roughly proportional to the winglet length (same as the rolling moment). Aircraft exhibiting "good" roll rates (according to the pilots) verify $\hat{p} \geq 0.07$ (Ref. 11). It appears then from figure 9 that only the long-winglet configuration with a fully deflected winglet at $C_{L_0} = 0.4$ will meet that quality criterion. That criterion can be relaxed to smaller values though, depending on the aircraft mission, so the concept could effectively be used at smaller C_{L_0} and/or with shorter winglets.

3. Trimmed turning flight

The long-winglet configuration was numerically analyzed in a turning airflow, simulating a steady level turn governed by the following algebraic equations:

$$V_{cg} = \sqrt{W/(1/2\rho C_{L_0} S)} \quad (3)$$

$$C_L = C_{L_0}/\cos\phi \quad (4)$$

$$R = V_{cg}^2/g\tan\phi \quad (5)$$

$$\Omega = V_{cg}/R \quad (6)$$

$$p = 0 \quad (7)$$

$$q = \Omega\sin\phi \quad (8)$$

$$r = \Omega\cos\phi \quad (9)$$

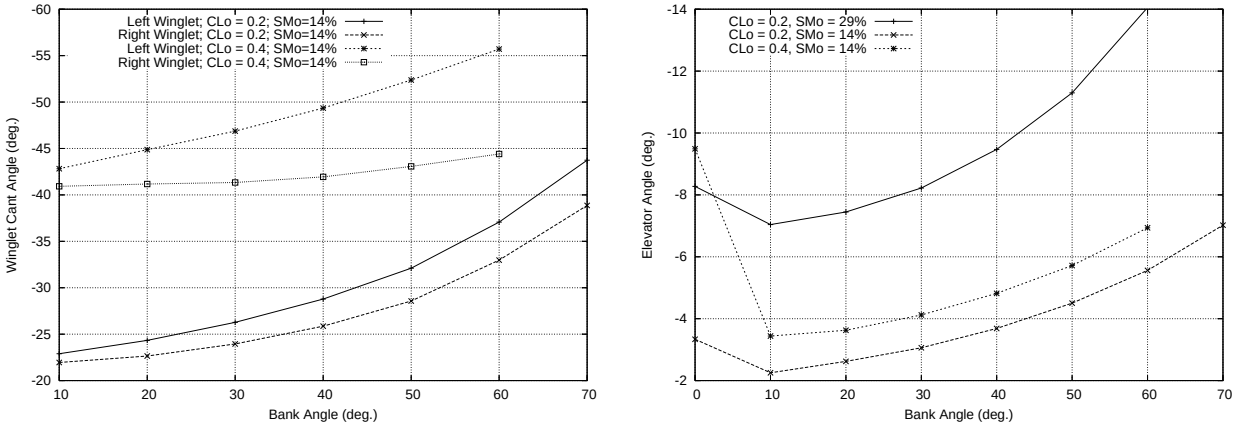

Figure 10. Control angles for the morphing flying wing to sustain a level turn at a given bank angle (VLM computations corrected for profile drag; C_{L_0} and SM_0 are respectively the lift coefficient and the static margin before entering the turn, at $\phi = 0$, when the wing was planar).

where C_{L_0} is the lift coefficient at zero bank angle, that is in straight level flight, before initiation of the turn. The rotation rates were directly constrained, given the bank angle and the turn rate. The sideslip angle was fixed to zero. The control angles, γ_l, γ_r, δ_e, required to zero out the aerodynamic moments during the turn[b], as well as the angle of attack required to maintain the lift coefficient prescribed from Eq. (4), are obtained by solving the following non-linear system (the non-linearity stems from the stability derivatives, which depend on the angles of attack and control), using an iterative technique (successive over relaxation):

$$\begin{pmatrix} C_{L_\alpha} & C_{L_{\delta_e}} & C_{L_{\gamma_l}} & C_{L_{\gamma_r}} \\ C_{l_\alpha} & C_{l_{\delta_e}} & C_{l_{\gamma_l}} & C_{l_{\gamma_r}} \\ C_{m_\alpha} & C_{m_{\delta_e}} & C_{m_{\gamma_l}} & C_{m_{\gamma_r}} \\ C_{n_\alpha} & C_{n_{\delta_e}} & C_{n_{\gamma_l}} & C_{n_{\gamma_r}} \end{pmatrix} \begin{pmatrix} \Delta\alpha \\ \Delta\delta_e \\ \Delta\gamma_l \\ \Delta\gamma_r \end{pmatrix} = \begin{pmatrix} C_L - C_L^\star \\ -C_l^\star \\ -C_m^\star \\ -C_n^\star \end{pmatrix} \tag{10}$$

where the starred quantities refer to the current guess of the constrained aerodynamic coefficients and where the stability derivatives are evaluated at the current operating point. The Δ's symbolize the correction to be added to the current (trial) values of angle of attack and control angles. Converged results for $C_{L_0} = 0.2\,;\, 0.4$ are plotted in figure 10 for different bank angles (i.e. different turn radii). The predicted winglet deflection angles are all negative, which means the winglets are deflected under the wing plane, and their magnitude increase with the bank angle and C_{L_0}. The right winglet (the one inside the turn) is less deflected than the left one, generating thus more lift so as to counter-act the induced roll (which would increase the bank angle during the turn otherwise); the deflection differential between left and right hand sides increases with the bank angle (smoothly at $C_{L_0} = 0.2$: from 4% difference at $\phi = 10^o$ to 12% difference at $\phi = 60^o$; but significantly at $C_{L_0} = 0.4$: from 5% difference at $\phi = 10^o$ to 25% difference at $\phi = 60^o$). At first the longitudinal position of the CG was fixed $0.76\,c_{root}$ aft of the wing apex (which corresponds to a static margin of 14% when the wing is planar), and all the computed, trimmed configurations were then statically stable in the turn. Relocating the CG closer to the wing apex, $0.65\,c_{root}$ behind it (which corresponds to a static margin of 29% when the wing is planar), did not alter significantly the computed winglet deflections but the elevator angle, which had to be more upward so as to balance the increased nose heaviness (see right-hand-side graph in figure 10). The setting of the elevator with increased bank angle is typical: the tighter the turn, the more up elevator is needed to keep the aircraft turning. However due to the favorable nose-up pitching moment created by the deflection of the winglets off the wing plane, the elevator burden is alleviated and there exists a range of bank angles for which one has to use down elevator (w.r.t. the elevator setting of the planar configuration in trimmed, straight, level flight); which means there is a particular bank angle for which no change in elevator angle is required (about 30^o at $\mathrm{SM}_0 = 14\%$ for both C_{L_0} investigated).

[b]Limiting ourselves to the case of small turn rates (i.e. $b \ll 2R$), and assuming the thrust line passes through the aircraft CG, aerodynamic moments about the aircraft CG are zero to the first order in rotation rates.

C. Application to longitudinal control and balance: winglets deflected in tandem

When moved in tandem, adaptive winglets allow to nose up or down the flying-wing airframe and/or to adjust it to a new longitudinal equilibrium state (i.e. flying at a different speed or climb/glide angle) without altering the lateral/directional balance. This capability in pitch control has been ascribed to the relocation of the aerodynamic centre that occurs whenever winglets mounted on a swept planform are moved around their root axis, while the chordwise position of the center of gravity remains the same. Hence pitch control with adaptive winglets is achieved through a dynamic static margin, which is in contrast with elevators which generate a control moment by altering the zero-lift pitching moment. Since deflecting the winglets (up or down) off the wing plane will only produce a nose-up pitching moment (w.r.t. the planar configuration, see figures 4 and 7), one has to pick a non-planar baseline configuration (say $\gamma = \gamma_l = \gamma_r = \pm 45^o$, see figure 11) to produce both nose-up and nose-down pitching moments w.r.t. that baseline when trimmed. Predicted and measured pitching moments relative to such a baseline are plotted in figure 12 for a cant angle sweep at fixed angle of attack and fixed elevator deflection. The VLM predictions give the right trend in a conservative way, since they under-estimate the experimental data. Nose-up pitching moments are obtained by folding the winglets more (bringing them closer to an upright position), nose-down pitching moments are created by unfolding the winglets (bringing them planar). Note that, with our arbitrarily-chosen reference deflection ($\pm 45^o$), generated nose-down pitching moments are slightly smaller than their nose-up counterparts. From the practical point of view, using down-deflected winglets may be better in terms of minimum actuation energy if we use the adaptive winglet concept as a means of trimming the aircraft longitudinally: unfolding the winglets creates a nose-down pitching moment at fixed angle of attack, hence the new trim flight point with unfolded winglets will be obtained at a smaller angle of attack, that is at a greater speed (smaller C_L), however increasing the flight speed means increasing the load on the winglets, so the aerodynamic forces will help to morph the aircraft in that case (by pulling the winglets upward). Similarly, deflecting more the down-winglets will allow to trim at a smaller flight speed, however slowing down the aircraft makes the folding operation easier because of reduced aerodynamic loads.

Computations of the angle of attack to trim the aircraft longitudinally were carried out for various winglet cant angles at fixed elevator deflection (which deflection was trimming the $\gamma = \pm 45^o$ configurations at $C_L = 0.2$). The same solution procedure as the one used to get the control angles during a turn was applied (in the present case, only the first two lines and columns of the matrix system (10) were taken into account). Results are plotted in figure 13 in terms of γ_{trim} vs C_L. Again, down winglets seem to be more beneficial, since they allow to reach greater C_L than up winglets (e.g. in the long-winglet case, at maximum deflection: C_L above 1.1 with down winglet and below 0.8 with up winglet). The long winglets allow to cover a broader, more practical, range of lift coefficients ($C_L \in [0.12; 1.13]$) than the short winglets do ($C_L \in [0.15; 0.47]$).

VI. Conclusion and Perspectives

The investigated concept of variable-cant-angle winglets appears to be a promising alternative to conventional control surfaces such as ailerons, elevators and rudders as far as basic manoeuvres are concerned. Numerical and experimental studies showed that such adaptive winglets enable control moments about multiple axes, forming then a highly coupled flight control system; this is in contrast with conventional control surfaces which form a decoupled control system. However, a single pair of adaptive winglets cannot substitute for all the conventional control surfaces at the same time if one wants to get a full control envelope. Indeed, numerical simulations showed us that one can achieve a trimmed level turn (i.e. pitching, rolling and yawing moments are zeroed out while in banked flight) with a single pair of adaptive winglets as sole control effectors, but only for a specific turn radius. To access a continuous range of turn radii with adaptive winglets as control effectors, one has then to combine their action with some elevators for instance. An alternative considered at the university of Bristol is to use a second pair of adaptive winglets on top of the first one to control the aircraft in pitch without elevators (see figure 14): with four independent multi-axis effectors, the system is then over-actuated, leading to some redundancy in the flight control system, which could be exploited to optimize secondary objectives (e.g. minimum drag, minimum bending moment) at fixed lift and moments.

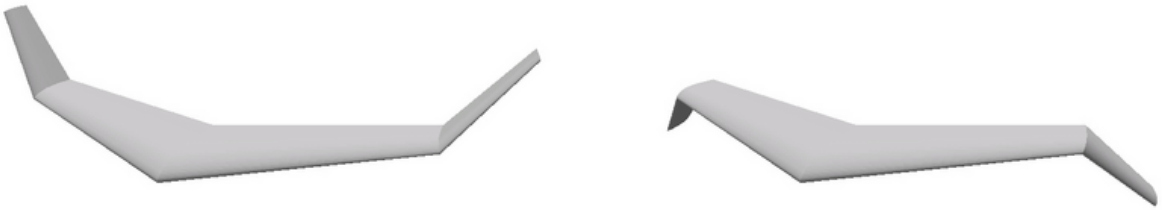

Figure 11. Baseline, symmetric configurations for pitch control.

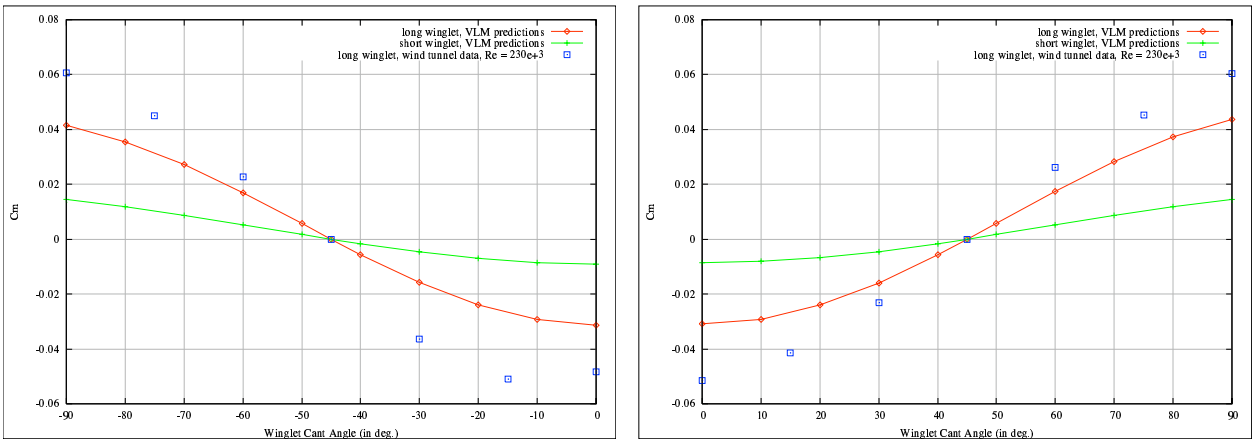

Figure 12. Pitching moments attainable by deflecting both winglets in tandem (numerical predictions with profile drag correction and experimental data; left: down-winglet case; right: up-winglet case). For both cases, the elevator angle and angle of attack were fixed during the (experimental and numerical) cant angle sweep, so as to trim the baseline configuration at $C_{L_0} = 0.2$ in straight level flight. Re is based on the root chord of the wing and on the speed at sea level corresponding to the prescribed C_{L_0}.

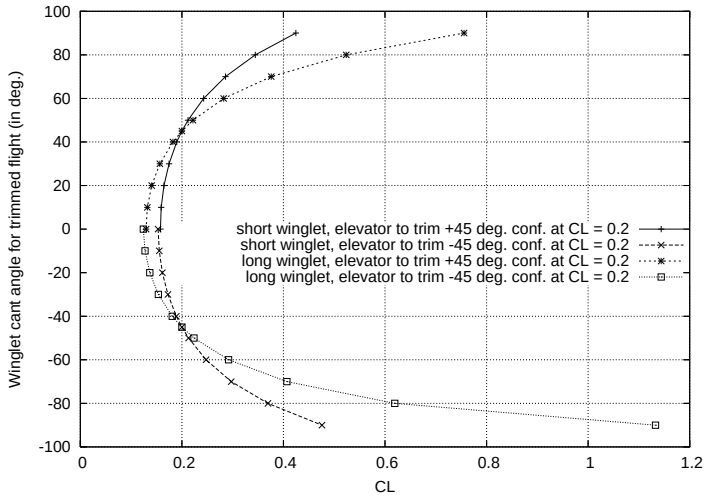

Figure 13. Cant angles to trim the aircraft longitudinally at different flight points (straight, level flights), winglets are moved in tandem, elevator angle is fixed so as to trim the $\gamma = \pm 45^o$ configurations at $C_L = 0.2$ (fixed value is not the same, slightly different though, for up- and down-winglet cases). Profile drag was not accounted for during the computations.

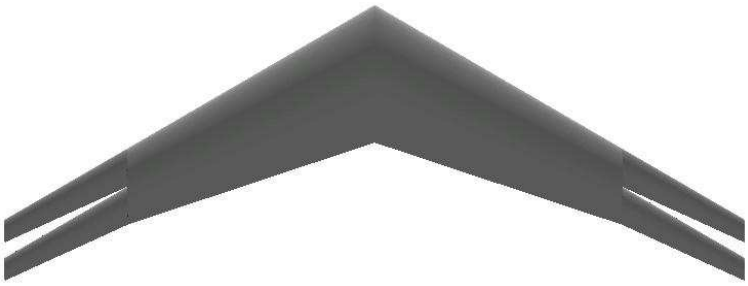

Figure 14. Flying wing configuration with four independent all-moving winglets as sole control effectors (top view, winglets undeflected).

Acknowledgments

This work has been supported by a Marie-Curie excellence research grant funded by the European Commission.

References

[1]Culick, F. E. C., "The Wright Brothers: First Aeronautical Engineers and Test Pilots," *AIAA Journal*, Vol. 41, No. 6, June 2003, pp. 985-1006.

[2]Jha, A. K., and KudvaSmart, J. N., "Morphing Aircraft Concepts, Classifications, and Challenges," Structures and Materials 2004: Industrial and Commercial Applications of Smart Structures Technologies, Proceedings of SPIE, Vol. 5388, pp. 213-224.

[3]Sanders, B., Eastep, F. E., and Forster, E., "Aerodynamic and Aeroelastic Characteristics of Wings with Conformal Control Surfaces for Morphing Aircraft," *Journal of Aircraft*, Vol. 40, No. 1, Jan.-Feb. 2003, pp. 94-99.

[4]Hall, J. M., "Executive Summary AFTI/F-111 Mission Adaptive Wing," WRDC-TR-89-2083, Sept. 1989.

[5]Khot, N. S., Zweber,J. V., Veley, D. E., Oz, H., and Eastep, F. E. "Flexible Composite Wing with Internal Actuation for Roll Maneuver," *Journal of Aircraft*, Vol. 39, No. 4, July-Aug. 2002, pp. 521-527.

[6]Natarajan, A., Kapania, R. K., and Inman, D. J., "Aeroelastic Optimization of Adaptive Bumps for Yaw Control," *Journal of Aircraft*, Vol. 41, No. 1, Jan.-Feb. 2004, pp175-185.

[7]Neal, D. A., Good, M. G., Johnston, C. O., Robertshaw, H. H., Mason, W. H., and Inman, D. J., "Design and Wind-Tunnel Analysis of a Fully Adaptive Aircraft Configuration," 45th AIAA/ASME/ASCE/AHS/ASC Structures, Structural Dynamics and Materials Conference, 19 – 22 April 2004, Palm Springs, California, AIAA 2004-1727.

[8]Bae,J., Seigler, T. M., Inman, D. J., and Lee, I., "Aerodynamic and Aeroelastic Considerations of A Variable-Span Morphing Wing," 45th AIAA/ASME/ASCE/AHS/ASC Structures, Structural Dynamics and Materials Conference, 19 – 22 April 2004, Palm Springs, California, AIAA 2004-1726.

[9]Henry, J. J., Blondeau J. E., and Pines, D. J., "Stability Analysis for UAVs with a Variable Aspect Ratio Wing," 46th AIAA/ASME/ASCE/AHS/ASC Structures, Structural Dynamics and Materials Conference, 18 – 21 April 2005, Austin, Texas, AIAA 2005-2044.

[10]Saffman, P. G., *Vortex dynamics*, Cambridge University Press, 1992.

[11]Raymer, D. P., *Aircraft design: a conceptual approach*, AIAA Education Series, 1989.